2015

Multiobjective Optimization of Switched Reluctance Motors Based on Design of Experiments and Particle Swarm Optimization

Cong Ma
University of Nebraska-Lincoln, cma9@unl.edu

Liyan Qu
University of Nebraska-Lincoln, lqu2@unl.edu

Year: 2015, Volume: PP, Issue: 99
Pages: 1 - 10, DOI: 10.1109/TEC.2015.2411677

Multiobjective Optimization of Switched Reluctance Motors Based on Design of Experiments and Particle Swarm Optimization

Cong Ma, *Student Member, IEEE*, and Liyan Qu, *Member, IEEE*

***Abstract*—This paper proposes a comprehensive framework for multiobjective design optimization of switched reluctance motors (SRMs) based on a combination of the design of experiments and particle swarm optimization (PSO) approaches. First, the definitive screening design was employed to perform sensitivity analyses to identify significant design variables without bias of interaction effects between design variables. Next, optimal third-order response surface (RS) models were constructed based on the Audze–Eglais Latin hypercube design using the selected significant design variables. The constructed optimal RS models consist of only significant regression terms, which were selected by using PSO. Then, a PSO-based multiobjective optimization coupled with the constructed RS models, instead of the finite-element analysis, was performed to generate the Pareto front with a significantly reduced computational cost. A sample SRM design with multiple optimization objectives, i.e., maximizing torque per active mass, maximizing efficiency, and minimizing torque ripple, was conducted to verify the effectiveness of the proposed optimal design framework.**

***Index Terms*—Design of experiments (DoE), multiobjective optimization, particle swarm optimization (PSO), response surface (RS), sensitivity analysis, switched reluctance motor (SRM).**

I. Introduction

SWITCHED reluctance motors (SRMs) have been used in many applications over the past few decades owing to their high robustness, low manufacturing cost, and simple structure. However, a relatively high torque ripple caused by the doubly salient pole structure is one of the primary disadvantages of SRMs. Much research has been conducted to reduce the torque ripples of SRMs via design optimization [1]–[4]. However, most existing designs targeted on single objective of torque ripple minimization, resulting in a relatively low average torque [5]. To improve the overall performance of SRMs, multiobjective optimization to maximizing the average torque while minimizing the torque ripple have been studied in SRM designs [2], [6]–[8]. Generally, the multiple objectives often conflict with each other and it is difficult to obtain the optimal solution. Moreover, an optimization processor was usually coupled with a finite-element analysis (FEA) solver for the machine design optimization, which has a high computational cost.

Manuscript received June 1, 2014; revised November 30, 2014; accepted March 2, 2015. Paper no. TEC-00398-2014.

The authors are with the Department of Electrical and Computer Engineering, University of Nebraska–Lincoln, Lincoln, NE 68588-0511 USA (e-mail: cma9@unl.edu; lqu2@unl.edu).

Color versions of one or more of the figures in this paper are available online at http://ieeexplore.ieee.org.

Digital Object Identifier 10.1109/TEC.2015.2411677

Design of experiments (DoE) [1]–[2], [7]–[12] and stochastic evolutionary methods [13]–[15] are two popular techniques employed for electric machine design optimization. DoE is a statistical method that effectively quantifies the effects of changes in design variables on machine responses. The one-factor-at-a-time (OFAT) method, a method of DoE, was used to optimize SRMs with only two design variables for electric vehicle applications [7]. The OFAT method will become impractical when more design variables are considered, because the number of experiments increases exponentially with the number of design variables. The problem can be mitigated by using advanced DoE, such as the central composite design (CCD) [8]–[11] and the Latin hypercube design (LHD) [12]. These methods have been utilized in the machine design optimization problems with up to five design variables [8]–[12]. In the CCD, the sample points are only distributed at the corner and center of the design space, which makes it difficult to efficiently gather the global machine response information within a wide design space. The LHD is a random sampling method that has the benefits of flexibility and a good space-filling property [16]. The number of experiments in the LHD is controllable. However, the sample points created by the LHD may poorly cover the design space. Stochastic evolutionary methods, such as genetic algorithm (GA) and particle swarm optimization (PSO) [17], are favorable in machine design optimization because they can search a high dimension of the design space in a computationally efficient manner [13]. The stochastic evolutionary methods have been coupled with an FEA solver to optimize the designs of SRMs [14]–[15]. However, due to the use of the computationally costly FEA solver, the overall computational costs of the combined approaches are intensive, especially for multiobjective optimization problems.

Recently, a new class of electric machine design optimization methods combining DoE and stochastic evolutionary methods is worth noting [18]–[21]. The methods reduced the computational cost of the traditional approaches coupling the FEA with stochastic evolutionary methods. In [18], the CCD was used to construct response surface (RS) models. Sensitivity analyses were then performed to identify the significant design variables based on the first-order regression coefficients of the RS models. However, the effects of the interactions between design variables were not considered when using the first-order regression coefficients as the sensitivity indices. After the sensitivity analysis, a differential evolutionary algorithm coupled with an FEA solver was used to find the optimal values of the selected significant design variables to optimize the machine design.

The computational cost of this optimization process is still high due to the use of the FEA for each candidate design. Instead of coupling with the FEA solver, evolutionary methods were coupled with RS models for optimization in [19]–[21], in which second-order (2nd-order) RS models were constructed by performing DoE and utilized to predict the machine responses during the optimization searching process. The elimination of FEA iterations in the search of the optimal designs effectively reduced the computational cost. However, the studies of the RS model-based optimization were limited to the problems with up to five design variables [22]. The electric machine design problems usually involve a large number of design variables. Therefore, it is necessary to investigate the possibility of the RS model-based optimization with more than five design variables. A limitation of the 2nd-order RS models is that their accuracy decreases with the increasing dimension of the design space, which may lead to incorrect optimal solutions. In addition, more samples will be required to cover the design space with a higher dimension for the construction of the RS models, and the distribution of the samples is important to the accuracy of the RS models. However, the samples obtained from a traditional CCD are proportional to the dimension of the design space. As a result, it may be inappropriate to use the CCD to solve the target problem. The number of the samples obtained from the LHD is controllable; however, the distribution of the samples should be carefully arranged to ensure the accuracy of the RS model. Therefore, two major issues in the traditional RS model-based methods need to be addressed: the accuracy of the RS models and the choice of an appropriate DoE.

This paper proposes a comprehensive framework for multiobjective design optimization of SRMs. Starting with a 6/10 SRM design problem with 14 independent design variables, a new class of small three-level designs, known as definitive screening designs (DSD), is employed to perform sensitivity analyses to identify the significant design variables without the bias of interaction effects between design variables. The number of design variables is reduced based on the sensitivity analyses. Next, to improve the accuracy of the RS models and the feasibility of DoE, optimal third-order (3rd-order) RS models are constructed by performing Audze–Eglais Latin hypercube designs (AELHD). The constructed optimal RS models consist of only significant regression terms, which are selected by using PSO. Then, a PSO-based multiobjective optimization is performed based on the constructed RS models, instead of the FEA of each candidate design, to generate the Pareto front [22] with significantly reduced computational cost. The optimal design can then be obtained from the Pareto front generated. A sample SRM design problem with multiple design objectives, which include maximizing torque per active mass, maximizing efficiency, and minimizing torque ripple, is solved using the proposed design optimization framework. The results, including the generated RS models, the Pareto front, and the optimal designs are compared with those obtained from the traditional optimal design methods using the 2nd-order RS models and an FEA solver to verify the high accuracy and low computational cost of the proposed design optimization framework.

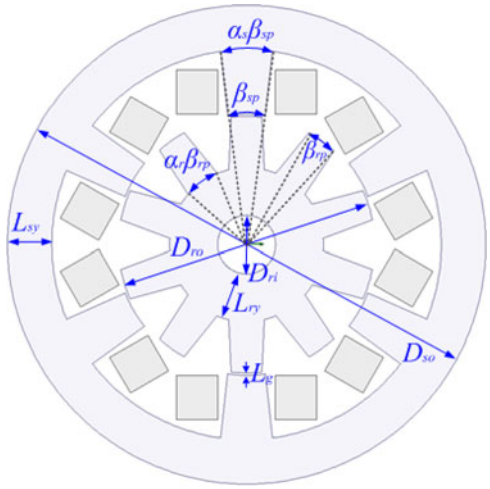

Fig. 1. Cross section of a 6/10 SRM.

TABLE I
INDEPENDENT DESIGN VARIABLES OF A 6/10 SRM

Design Variable	DEFINITION
D_{ri}	Inner diameter of rotor
D_{ro}	Outer diameter of rotor
D_{so}	Outer diameter of stator
L_g	Length of airgap
L_{ry}	Length of rotor yoke
L_{sy}	Length of stator yoke
L_{stk}	Stack length
β_{rp}	Rotor pole arc angle at airgap
β_{sp}	Stator pole arc angle at airgap
α_s	Ratio between stator pole arc at stator back iron and stator pole arc at airgap
α_r	Ratio between rotor pole arc at rotor back iron and rotor pole arc at airgap
D_w	Diameter of copper wire
I_c	Chopping current
N_t	Number of turns per pole

II. SRM DESIGN SPECIFICATIONS AND OPTIMIZATION

The relatively simple structure of SRMs makes their designs less complex than other ac or dc machine designs. However, in order to precisely determine the machine geometric structure, there are still ten independent design variables to be considered for the cross section of a 6/10 SRM, as shown in Fig. 1. In addition, the stack length L_{stk}, the chopping current I_c, and two winding design variables comprising the number of turns per pole, N_t, and the diameter of copper wire, D_w, are considered. Therefore, the total number of independent design variables is 14, as listed in Table I. The major design specifications are listed in Table II. The type of ferromagnetic material used for the stator and rotor laminations is M19 steel (29 gauge). The SRM is assumed to be operated with a unipolar current excitation [23].

The design optimization of an SRM begins with the definition of the optimization model, which includes design variables, design constraints, and design objectives. In order to meet the

TABLE II
DESIGN SPECIFICATIONS OF THE SRM

Rated speed	1 500 r/min
Rated torque	9.49 Nm
Rated power	2 hp
Efficiency	$>$ 85% at rated speed
Torque ripple	$<$ 35%
Mounting	NEMA 143 (Outer diameter 139.7mm)

design requirements and achieve the optimal performance of the SRM, three objectives, i.e., minimum torque ripple, maximum efficiency, and maximum torque per active mass, are selected for the multiobjective design optimization in this paper. The torque ripple T_r is defined as

$$T_r = \frac{T_{\max} - T_{\min}}{T_{\text{avg}}} \tag{1}$$

where $T_{\max}$, $T_{\min}$, and T_{avg} are the maximum, minimum, and average torque, respectively. The efficiency η of an SRM is estimated considering only core and copper losses

$$\eta = \frac{T_{\text{avg}}\omega}{T_{\text{avg}}\omega + P_{\text{core}} + P_{\text{cu}}} \tag{2}$$

where ω is the rotational speed, P_{core} is the core loss, and P_{cu} is the copper loss. To increase the torque output of the SRM while reducing the machine weight (or the material cost), the average torque per active mass T_m is considered

$$T_m = \frac{T_{\text{avg}}}{m_{\text{Cu}} + m_{\text{Fe}}} \tag{3}$$

where m_{Cu} and m_{Fe} are the masses of the copper wire and steel of the motor, respectively.

The optimization is subjected to the following constraints.

1) The average flux densities in the stator and rotor poles at the aligned positions, B_{sp} and B_{rp}, should meet to following constraints to avoid significant saturation:

$$B_{\text{sp}} \le B_{\text{sat}} \text{ and } B_{\text{rp}} \le B_{\text{sat}} \tag{4}$$

where B_{sat} is the saturation magnetic flux density of the steel.

2) The current density *J* is limited due to the thermal constraints, which limit the operating temperature of the SRM

$$J \le J_{\text{Max}} \tag{5}$$

where $J_{\max}$ is the maximum current density. The value of $J_{\max}$ can be determined from the maximum copper loss $P_{\text{cu}}(P_{\text{cu}} = J_{\max}^2 \pi D_w^2 R/4)$ that can be dissipated during the SRM operation without exceeding the maximum winding temperature, where *R* is the winding resistance. The maximum copper loss P_{cu} is determined by the heat convection equation $P_{\text{cu}} = h_c A \Delta T$, where h_c is the convective heat transfer coefficient, which can be calculated using the method in [24], *A* is the heat transfer area, and ΔT is the difference between the maximum winding temperature and the ambient temperature.

3) The stator slot space includes the net available space for the copper wires plus slot lining or insulation. Usually, the fill factor k_{fill} is constrained by

$$30\% \le k_{\text{fill}} \le 60\%. \tag{6}$$

4) For the 6/10 SRM with a higher number of rotor poles, the ratio α_r should satisfy the geometrical limitation for the pole configurations, which can be described as

$$\alpha_r \le \frac{2\pi}{N_r \beta_{\text{rp}}} \tag{7}$$

where $N_r (= 10)$ represents the number of rotor poles.

Then, the optimization model can be formulated as follows, where the objective function is expressed as a weighted sum of individual objectives:

$$\min z(\boldsymbol{x}) = \quad w_1 \frac{T_r}{T_r'} + w_2 \frac{\eta'}{\eta} + w_3 \frac{T_m'}{T_m} \tag{8}$$

$$\text{subject to :} \quad (4) - (7) \tag{9}$$

$$\underline{x_i} \le x_i \le \bar{x}_i, i = 1, 2, ..., 14 \tag{10}$$

where $\boldsymbol{x} = [D_{\text{ri}}, D_{\text{ro}}, D_{\text{so}}, L_g, L_{ry}, L_{sy}, L_{\text{stk}}, \alpha_r, \alpha_s, \beta_{\text{rp}}, \beta_{\text{sp}}, D_w, I_c, N_t]$ is the vector of design variables; w_1, w_2, w_3 are weight factors satisfying $w_1 + w_2 + w_3 = 1$; T_r', η' and T_m' are the base values; and $\underline{x_i}$ and $\overline{x_i}$ are the lower and upper bounds of each design variable, respectively.

The aforementioned design optimization model has a high dimension design space. In the traditional optimal design approaches, the constraints (1)–(4) and objective function (8) were evaluated using an FEA solver for each candidate design, which makes the process of finding the optimal solution of the SRM design problem computationally intensive. To solve this problem, this paper proposes two methods: 1) design space reduction; and 2) using a surrogate model to replace the FEA solver to evaluate the constraints in the process of searching the optimal solution. In the next section, an optimization framework, which consists of sensitivity analysis-based design space reduction, optimal RS model construction, and PSO-based Pareto optimization, is proposed to solve the multiobjective optimization problem with a high-dimension design space.

III. PROPOSED COMPREHENSIVE FRAMEWORK FOR MULTIOBJECTIVE DESIGN OPTIMIZATION OF SRMS

This section proposes a comprehensive framework for multiobjective design optimization of an SRM, as shown in Fig. 2. The proposed framework begins with the optimization model (8)–(10), and is followed by three main parts described in the following sections: design space reduction through sensitivity analyses, construction of the optimal 3rd-order RS models, and PSO-based multiobjective optimization coupled with the constructed RS models.

A. Sensitivity Analysis for Design Space Reduction

To reduce the computational cost required for the optimization, sensitivity analyses are performed first to reduce the number of design variables. Sensitivity analyses can also provide

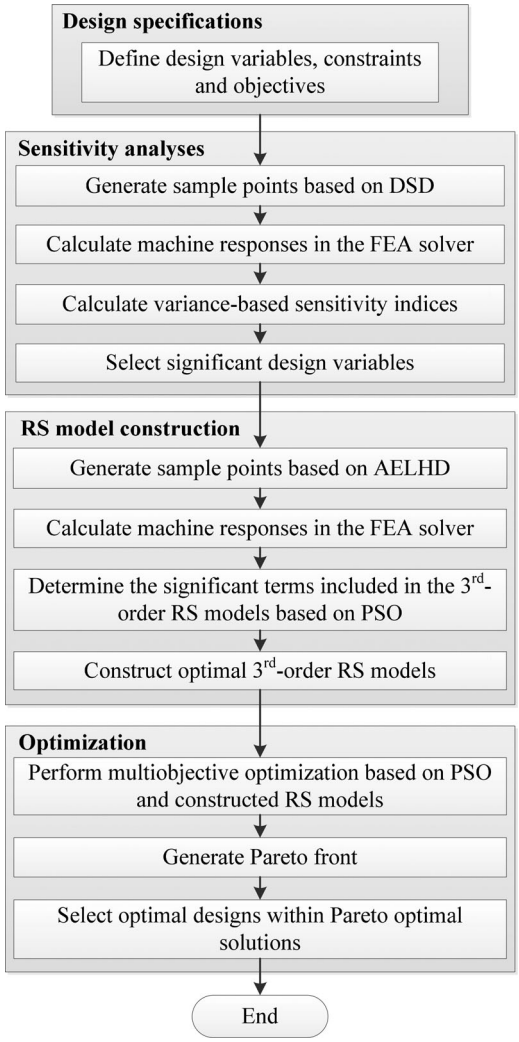

Fig. 2. Flow chart of the proposed multiobjective design optimization framework.

important insights on how each design variable affects the machine performance. Traditionally, local sensitivity analyses were performed through the OFAT experiments for SRMs in [25]–[27]. However, these methods neither measured the sensitivities quantitatively nor considered the interaction effects between design variables. The RS model-based sensitivity analyses discussed in [18] did not consider the interaction effects either by using the first-order regression coefficients as the sensitivity indices. In this paper, a variance-based sensitivity analysis approach is used to quantitatively measure the sensitivities of the machine responses to each design variable.

The variance-based sensitivity analysis is a global sensitivity analysis technique that quantitatively measures the contribution of each variable to the machine responses [28]. No partial derivatives or RS models are required. In order to examine the variance in the machine responses, experiments need to be designed and conducted to examine the design variables at different levels. For example, in a three-level design, the values of each variable are set at its minimum, medium, and maximum values within its limits. A well-designed experiment can greatly reduce the number of experiment runs without sacrificing the accuracy of the sensitivity analysis. In this paper, the sensitivity analysis is performed using the DSD. The DSD is a new class of three-level design capable of capturing nonlinearity and guarantees that the sensitivity indices of each design variable are unbiased by the interaction effects between design variables [29]. Moreover, the number of experiment runs is low, even if all of the independent design variables are considered at the beginning. Specifically, for a DSD with N design variables, only $2N+1$ experiment runs are required, which is much lower than 2^N+2N+1 required by the CCD [2]. The DSD can greatly reduce the computational cost of the sensitivity analysis. In this paper, the DSD is employed to test 14 independent design variables of SRMs, and only 29 experiments (compared to 16 413 for the CCD) need to be performed. The experiments were run in an FEA solver to calculate the machine responses, and the variance is calculated based on the simulation results. The sensitivity is measured by a sensitivity index that reflects the relative importance of the variable alone and is described as follows [28]:

$$S_{x_i} = \frac{V_{x_i}(E_{x_{\sim i}}(y|x_i))}{V(y)} \tag{11}$$

where $E_{x_{\sim i}}(y|x_i)$ is the average of y taken over $x_{\sim i}$ (all factors except for x_i) when x_i is fixed, $V_{x_i}(E_{x_{\sim i}}(y|x_i))$ is the conditional variance of $E_{x_{\sim i}}(y|x_i)$, and $V(y)$ is the variance of y. A higher sensitivity index indicates a larger influence to y by x_i.

The variance-based sensitivity indices of the three machine responses, T_r, η, and T_m, to the 14 design variables are evaluated and the results are shown in Fig. 3. According to Fig. 3, $D_{\rm ro}$, D_w, I_c, L_g, $L_{\rm stk}$, N_t, $\beta_{\rm sp}$, and $\beta_{\rm rp}$ are significant design variables for the SRM optimization. The changes in other design variables $D_{\rm ri}$, $D_{\rm so}$, L_{ry}, L_{sy}, α_r, and α_s have negligible effects on any of the three responses. The values of the insignificant design variables can be determined based on other design considerations, or can be set at the levels where the optimal responses are obtained from the sensitivity analyses. For example, α_s can be set to a relatively large level to ameliorate vibration [30]; the stator outer diameter $D_{\rm so}$ is predetermined by the geometrical constraint of the mounting frame. These insignificant design variables are not selected as design variables and become constants in the subsequent optimization process. In addition, a significant design variable, chopping current I_c, is determined by the nominal condition of the SRM and becomes a constant in the optimization process as well. Therefore, the number of independent design variables in the following design optimization process is reduced from 14 to 7. In other words, the dimension of the design space is reduced, and the reduced design variables can be expressed as $\boldsymbol{x}_r = [D_{\rm ro}, L_g, L_{\rm stk}, \beta_{\rm rp}, \beta_{\rm sp}, D_w, N_t]$. In this paper, the forced air cooling is used for the SRM, the maximum winding temperature is 150 °C and the ambient temperature is 25 °C. According to the discussion of the constraint 2) in Section II, the maximum current density is calculated to be 7 A/mm^2. All design variables, constants, and their values or ranges for optimal design of the 6/10 SRM are listed in Table III.

An initial design of the SRM is obtained based on the results of the sensitivity analyses and the designer's experience. In the initial design, the seven important design variables are

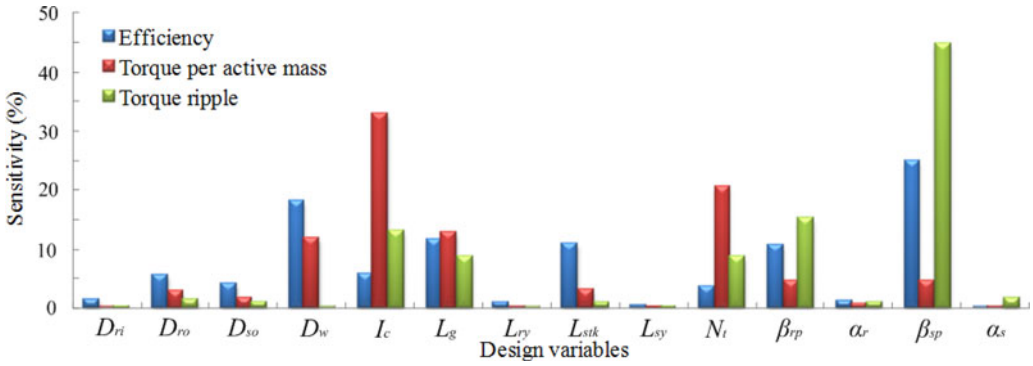

Fig. 3. Sensitivity indices of torque ripple, efficiency, and torque per active mass to the 14 design variables for a 6/10 SRM.

TABLE III
VARIABLES AND CONSTANTS FOR THE OPTIMAL DESIGN OF THE 6/10 SRM

Design Parameter	Type	Unit	Value
$D_{\rm ro}$	Variable	mm	60.0–85.0
D_w	Variable	mm	0.912–1.628
L_g	Variable	mm	0.30–0.75
$L_{\rm stk}$	Variable	mm	40.0–90.0
N_t	Variable	N/A	40–90
$\beta_{\rm rp}$	Variable	deg	14.0–19.0
$\beta_{\rm sp}$	Variable	deg	14.0–20.0
$D_{\rm ri}$	Constant	mm	17
$D_{\rm so}$	Constant	mm	139.7
L_{ry}	Constant	mm	16.5
L_{sy}	Constant	mm	15
I_c	Constant	A	15
α_r	Constant	N/A	1.98
α_s	Constant	N/A	1.05
$B_{\rm sat}$	Constraint	T	1.65
$J_{\rm max}$	Constraint	A/mm^2	7
$k_{\rm fill}$	Constraint	N/A	30%–60%

determined as follows: $D_{\rm ro}$, $L_{\rm stk}$, and L_g are set at the levels where the best responses are achieved among the three levels of these variables in the sensitivity analyses; N_t, $\beta_{\rm rp}$, and $\beta_{\rm sp}$ are first set at the best levels obtained from the sensitivity analyses, and then, are adjusted to avoid significant saturation and maintain a wide unaligned position of the SRM, as discussed in [31] and [32]; and D_w is determined by the available space in the stator slots and N_t.

B. Constructing the Optimal RS Models

After sensitivity analyses, the RS models are constructed by performing the DoE. In order to replace the FEA solver with the RS models in the optimization searching process, the RS models should accurately predict the machine responses. The accuracy of the RS models highly depends on both the DoE and the form of the RS models.

In this paper, the AELHD is employed to ensure a uniform space filling within the whole design space [33]. The AELHD distributes the experimental points as uniformly as possible by minimizing the potential energy $E_{\rm AE}$ between the points

$$E_{\rm AE} = \sum_{i=1}^{N_p} \sum_{j=i+1}^{N_p} \frac{1}{L_{ij}^2} \tag{12}$$

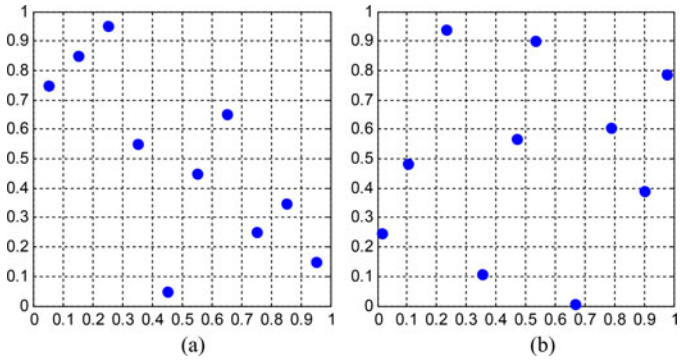

Fig. 4. Examples of (a) LHD and (b) AELHD for a problem with two design variables of ten levels.

where N_p is the number of experimental points in the AELHD and L_{ij} is the Euclidean distance between points i and j. The comparison between the traditional LHD and the AELHD for a simple case with two design variables of ten levels is shown in Fig. 4. It can be seen that the AELHD has a better space-filling performance than the traditional LHD. In addition, the quality of AELHD depends on the number of experiments N_p. In this paper, a medium-size AELHD [34] is employed. The number of experiments for a medium-size design is twice the number of regression terms in a full 3rd-order model. Therefore, for the design optimization problem with $N = 7$ design variables, an AELHD with 240 experiments is performed to construct the RS models. In this study, the machine responses of T_r, η, T_m, $B_{\rm sp}$, and $B_{\rm rp}$ are calculated in the FEA solver for each experiment, and are then used to construct the RS models.

Traditionally, 2nd-order RS models were usually applied to machine design problems with up to five selected design variables. As described in [22], the 2nd-order RS model did not converge even when a large number of experiments were used to build up the model. For the optimization problem with seven selected design variables in this paper, an optimized 3rd-order RS model is proposed to improve the approximation accuracy of the RS models. In the literature, the RS models higher than 2nd order were rarely discussed due to the following reasons. First, a 2nd-order RS model is usually accurate enough for most problems [35]. Second, RS models were generally applied to nondeterministic problems with noticeable random errors.

In these problems, the responses may differ for the same combination of design variables due to stochastic errors, and the accuracy of the approximation is not the sole goal. However, for the machine design problems which are deterministic, the accuracy of RS models is highly desirable. A full 3rd-order RS model can be expressed as

$$f(x) = a_0 + \sum_{i=1}^{N} a_i x_i + \sum_{i=1}^{N}\sum_{j\geq i}^{N} a_{ij} x_i x_j + \sum_{i=1}^{N}\sum_{j\geq i}^{N}\sum_{k\geq j}^{N} a_{ijk} x_i x_j x_k + \varepsilon \quad (13)$$

where a_0, a_i, a_{ij}, and a_{ijk} are the regression coefficients and ε is an error term. Compared with a full 2nd-order RS model with $1 + N + N(N+1)/2$ regression coefficients, the number of regression coefficients in the full 3rd-order RS model is increased significantly to $1 + N + N(N+1)/2 + N(N+1)(N+2)/6$. For example, when $N = 7$, there are 36 and 120 regression coefficients, respectively, in the 2nd-order and 3rd-order RS models. The number of regression coefficients in the 3rd-order RS model increases rapidly as *N* increases. As a result, the number of experiments and the computational cost required to determine these coefficients increase significantly. To reduce the size of the 3rd-order RS model, the terms that have negligible contributions to the response can be omitted from the model; and the RS model can be represented by the combination of the significant regression terms only. The reduction of the size of the 3rd-order RS model can reduce the computational effort in the optimization process without sacrificing the accuracy and the number of experiments required to determine the values of regression coefficients. This paper proposes a method to automatically select significant regression terms to be included in the 3rd-order RS model. The proposed method is based on PSO and consists of two steps explained as follows.

1) Define an Objective (Fitness) Function and Constraints: The fitness of a candidate RS model is evaluated based on two metrics: the quality of approximation of the experimental data by the candidate model and the size of the candidate model. The quality of the model is quantified by calculating the coefficient of determination R^2 [35]

$$R^2 = 1 - \frac{\sum_{i=1}^{N_p}(y_i - f_i)^2}{\sum_{i=1}^{N_p}(y_i - \bar{y})^2} \quad (14)$$

where y_i is the desired value obtained from FEA, f_i is the value predicted by the RS model, and $\bar{y}$ is the mean value of y_i. R^2 is an indicator of how well the RS model approximates the experimental data points. The better the model fits the data, the closer the value of R^2 is to one. The size of the model is measured in terms of the number of regression terms, N_r, in the model. Then, the objective function is formulated as

$$\min z_{\mathrm{RS}} = w\frac{N_r}{N_r'} + (1-w)\frac{R^{2'}}{R^2} \quad (15)$$

$$\text{subject to: } 36 \leq N_r \leq 120 \quad (16)$$

where *w* is the weighting factor, and R^2' and N_r' are the base values.

2) Perform the Optimization Using PSO: The PSO is applied to solve the optimization problem (15)–(16). PSO is a population-based stochastic optimization technique suitable for solving multiobjective optimization problems. It uses a population of particles to perform a multidirectional search for the optimal solution in the problem space. Each particle has a position P_k (i.e., N_r in this problem) representing a candidate solution in the design space defined by (16). The PSO algorithm is implemented iteratively to search for the optimal position according to the fitness evaluation using (15). In each iteration, once the value of N_r is determined for a particle, the coefficients of all 1st-order and 2nd-order terms and $(N_r - 36)$ 3rd-order regression terms are then determined using the least-square method to construct the RS model. Then, the fitness value Z_{RS} of each particle is calculated by using (15) and the constructed RS model. The fitness function values are then used in the PSO searching process to find the optimal value of N_r, based on which the optimal set of coefficients of (13) can be obtained using the least-square method to construct an optimal RS model. The optimal RS models of T_r, η, T_m, B_{sp}, and B_{rp} are built using the proposed method. The constructed optimal RS models are used to calculate the values of T_r, η, T_m, B_{sp}, and B_{rp} analytically for the multiobjective optimization. This eliminates the use of a computationally intensive FEA solver to estimate these quantities numerically in the process of searching the optimal solution.

C. Multiobjective Design Optimization for SRM

After the sensitivity-based design space reduction and optimal RS model construction, the optimization model (8)-(10) can be simplified as follows:

$$\min_x z(x_r) = w_1\frac{T_r(x_r)}{T_r'} + w_2\frac{\eta'}{\eta(x_r)} + w_3\frac{T_m'}{T_m(x_r)} \quad (17)$$

$$\text{subject to: } (4)-(7) \quad (18)$$

$$\underline{x}_{ri} \leq x_{ri} \leq \bar{x}_{ri}, \quad i = 1, 2, \ldots, 7 \quad (19)$$

Compared to the original optimization model (8)–(10) with 14 design variables, in the problem (17)–(19), the dimension of the design space has been reduced to 7 and the optimal 3rd-order RS models, instead of the FEA solver, are used to calculate T_r, η, and T_m in (17) and B_{sp}, and B_{rp} in (18). Next, the constrained optimization problem is converted to the following form by using the Lagrangian relaxation technique [36],

$$\min_x z(\boldsymbol{x}_r) = w_1\frac{T_r(\boldsymbol{x}_r)}{T_r'} + w_2\frac{\eta'}{\eta(\boldsymbol{x}_r)} + w_3\frac{T_m'}{T_m(\boldsymbol{x}_r)} + p(\boldsymbol{x}_r) \quad (20)$$

$$\text{subject to: } (19)$$

where $p(\boldsymbol{x}_r)$ is the penalty function for constraints (4)–(7). A larger penalty function value indicates a poor design that violates the constraints more severely. If all of the constraints are

TABLE IV
COMPARISON OF THE RESPONSE SURFACES WITH DIFFERENT DOE

RS models		2nd-order by CCD (143)	2nd-order by AELHD (143)	2nd-order by AELHD (720)	3rd-order by AELHD (240)
R^2	T_r	0.8831	0.9165	0.9256	0.9782
	η	0.9853	0.9934	0.9967	0.9993
	T_m	0.9845	0.9970	0.9980	0.9997
RMSE	T_r	0.1014	0.0926	0.0910	0.0889
	η	0.0349	0.0309	0.0295	0.0275
	T_m	0.0867	0.0801	0.0780	0.0752

satisfied, the value of $p(\boldsymbol{x}_r)$ is zero. The model (19) and (20) will be used for multiobjective SRM design optimization.

One of the challenges of multiobjective optimization is that the objectives usually conflict with each other and no unique solution can be found. In this paper, the Pareto optimality [22] is utilized to manage the tradeoffs among different objectives. Pareto optimal solutions are defined as a set of feasible solutions that cannot be improved without deteriorating other objectives. The Pareto front, which includes all Pareto optimal solutions, can provide a clear view of how much penalty is induced by the improvement of another objective. The generation of the exact Pareto front can be computationally intensive. In this paper, a PSO algorithm is adopted to search efficiently for the Pareto optimal designs within the design space based on (19) and (20). The process of finding the optimal solution includes three steps. First, define N_w different combinations of the three weighting factors in (20). Next, the PSO is adopted to search for the optimal solution of (20) with each set of weighting factors; and N_w optimal solutions corresponding to N_w sets of weighting factor combinations are obtained. Finally, all of the Pareto optimal solutions are used to approximate the Pareto Front for the design problem, from which the final optimal solution can be obtained.

IV. SIMULATION RESULTS

The design optimization of the SRM is performed using the proposed optimization framework. This section verifies the proposed method by using two statistical criteria as well as a direct comparison of the machine responses predicted by the proposed method and calculated by an FEA solver.

A. Accuracy of the Proposed Optimal RS Models

In this section, the accuracy of the 3rd-order RS models constructed by using the proposed method is compared with the traditional 2nd-order RS models using two statistical criteria: the coefficient of determination R^2 and the root-mean-square error (RMSE). As described in Section III-B, the quality of the RS model can be quantified by R^2. First, the 2nd-order RS models are constructed using the traditional CCD and the AELHD, respectively, with the same number of experiments (143 experiments). The qualities of the 2nd-order models constructed by the two different methods in terms of R^2 are compared in Table IV. The results show that the 2nd-order RS models constructed using the AELHD have higher R^2 (closer to one), meaning a better approximation of the experimental data by the models. Next, the 2nd-order RS models are constructed using the AELHD with a higher number of experiments (720 experiments) generated using the algorithm described in [34], representing a large-size design. Table IV shows that the quality of the approximation of the experimental data by the 2nd-order models has only been improved slightly using a large-size design. Particularly, the R^2 of the 2nd-order model of the torque ripple is only 92.56% even with the large-size design. This means that only 92.56% of the total variation can be represented by the model. Therefore, the 2nd-order RS models are not suitable for the optimization problem even with a high-dimension design space. Then, the proposed optimal 3rd-order RS models are constructed using the AELHD with a medium-size design (240 experiments). Table IV shows that the optimal 3rd-order RS models have the best approximation for the experimental data indicating by higher $R^2 s$ compared to the 2nd-order models constructed using different DoE. Specifically, the accuracy of the approximation for torque ripple response by the optimal 3rd-order model is much higher than that of the best 2nd-order model. Therefore, the relationship between the responses and the design variables can be more accurately represented by the optimal 3rd-order RS models.

To evaluate the approximation accuracy of the RS models within the whole design space, the following RMSE is defined:

$$\mathrm{RMSE} = \sqrt{\frac{1}{n}\sum_{i=1}^{n}(y_i - f_i)^2} \tag{21}$$

where n is the number of test points, which are randomly generated within the design space and were not used for constructing the RS models. Table IV also compares the RMSEs of different RS models. Lower values of the RMSE indicate less prediction errors of the RS models. From the comparison, the RMSE values of all the responses produced by the proposed 3rd-order models are all the lowest ones among different RS models. These results verified the improved fitness of the proposed 3rd-order models over the traditional 2nd-order models.

B. Accuracy and Computational Efficiency of the Proposed Method

After evaluating the accuracy of the proposed RS models using the statistical criteria R^2 and RMSE, the accuracy and computational efficiency of the proposed method are further compared with the traditional design optimization methods. Based on the 3rd-order RS models, the Pareto front is generated efficiently by solving (19)-(20) using the PSO. The PSO is designed to have a population size of 35 and the maximum iteration of 1000. The value of N_w is chosen to be 20. The Pareto optimal solutions with high efficiency, low torque ripple, and high torque per active mass are represented by the Pareto front shown in Fig. 5.

To evaluate the accuracy of the Pareto front obtained by the proposed method, two other Pareto fronts are generated for comparison. One is generated as a benchmark by using the PSO coupled with an FEA solver; the other is generated by using the

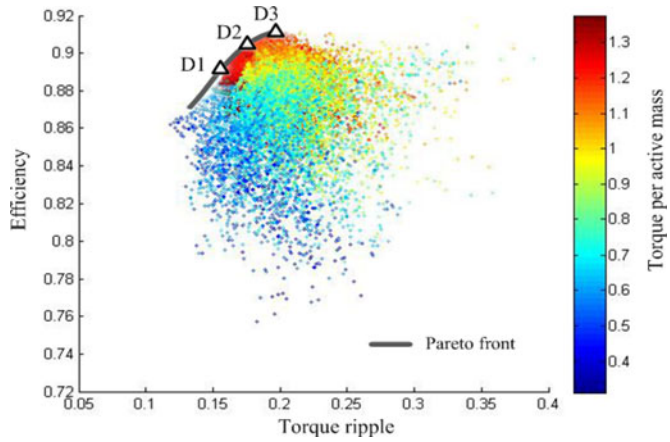

Fig. 5. Pareto front of the multiobjective optimization obtained from the proposed 3rd-order RS model-based method.

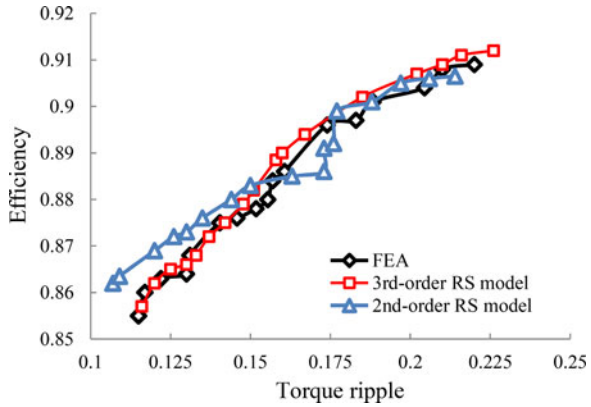

Fig. 6. Comparison of the Pareto fronts obtained by a PSO and FEA coupled method, a PSO and 2nd-order RS model coupled method, and the proposed PSO and 3rd-order RS model coupled method.

PSO coupled with the 2nd-order RS model obtained from the AELHD with 720 experiments. Fig. 6 compares the three Pareto fronts. The results show that the Pareto front obtained by the optimal 3rd-order RS model matches the benchmark Pareto front better than that obtained by the 2nd-order RS model. Moreover, the number of FEA iterations performed throughout the optimization process of the proposed method is only 240, which is much lower than 4 131 FEA iterations involved in the benchmark case combining the PSO and FEA. During the optimization process, the FEA iterations are the most time-consuming part. The proposed method greatly reduces the number of FEA iterations, and therefore, greatly reduces the computational cost and time. Specifically, in this case study, the optimization performed by the proposed method takes only several hours, which are much less than a few days taken by the PSO and FEA-coupled optimization on a same personal desktop computer with Intel core i7-3770 and 6 GB memory. The results show that the proposed optimization framework is capable of obtaining more accurate Pareto optimal solutions than the traditional 2nd-order RS model-based method and can obtain the Pareto optimal solutions more efficiently than the traditional FEA solver-based method without sacrificing the accuracy.

TABLE V
COMPARISON OF THE OPTIMAL DESIGNS

	Term	Initial design	D1	D2	D3
D_{ro} (mm)		80.00	79.97	80.00	80.00
D_w (mm)		1.151	1.151	1.290	1.369
L_g (mm)		0.30	0.30	0.30	0.30
L_{stk} (mm)		90.00	86.20	86.94	90.00
N_t		80	90	90	90
β_{rp} (deg)		15.00	16.38	15.70	15.21
β_{sp} (deg)		16.00	15.30	14.71	14.29
k_{fill}(%)		50.96	45.92	52.89	59.81
T_r (%)	RS	N/A	16.70	18.36	20.92
	FEA	25.12	18.30	20.13	24.38
η(%)	RS	N/A	89.40	90.31	90.95
	FEA	89.50	88.70	89.37	90.00
T_m (Nm/kg)	RS	N/A	1.371	1.350	1.332
	FEA	1.251	1.370	1.348	1.331

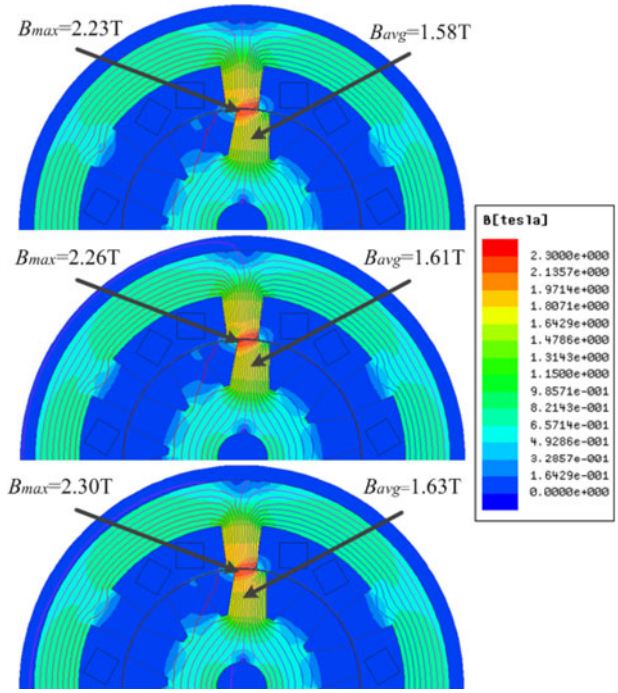

Fig. 7. Flux and field distributions of the three optimal designs in the nominal condition (upper: D1, medium: D2, and lower: D3).

C. Performance of the Optimal SRMs

To further evaluate the effectiveness of the Pareto optimal solutions obtained by the proposed method, four candidate designs, i.e., the initial design based on the sensitivity analyses and three optimal designs D_1, D_2, and D_3 selected from the Pareto front obtained by the proposed 3rd-order model shown in Fig. 5, are compared in Table V. For the initial design, the machine responses T_r, η, and T_m are calculated by the FEA solver. While for the three optimal designs obtained from the proposed method, the machine responses are calculated by the proposed RS models and the FEA solver, respectively. Table V shows that the initial design has the worst performance among the four cases. For example, T_r and T_m of D_1 are improved by

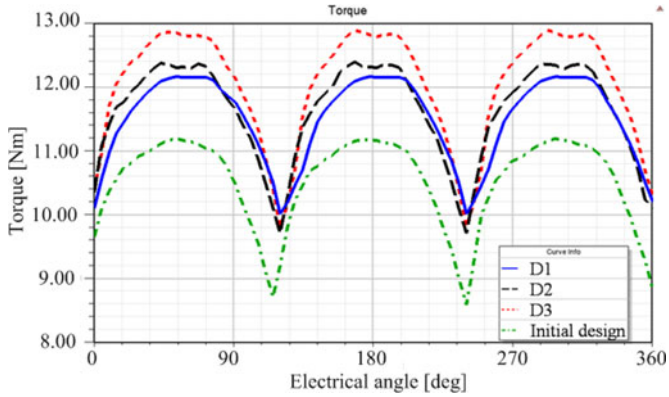

Fig. 8. Comparison of torque performance of the three optimal SRMs and the SRM obtained from the initial design.

27.15% and 9.51%, respectively, while η is 0.89% lower than those of the initial design. In addition, the machine responses calculated by the proposed RS models match well with those calculated by the FEA solver. As in Table V, D_1 has the lowest torque ripple, the highest torque per active mass, and the lowest efficiency as indicated by the Pareto front shown in Fig. 5. D_3 has the highest efficiency, the highest torque ripple, and the lowest torque per active mass. A tradeoff among these three design objectives exists and an optimal design can be selected based on the designer's preference.

Fig. 7 shows the flux and field distributions of the three optimal designs, where $B_{\max}$ is the maximum flux density in the pole tips and B_{avg} is the average flux density in the poles. It shows that the designed SRMs operate near the knee points at the nominal conditions. The torque waveforms of the four designs in the nominal condition are compared in Fig. 8, and the average torque of the initial design is lower than the optimal designs. These results verified that the optimal designs can be obtained by the proposed method effectively.

V. Conclusion

This paper proposed a comprehensive framework of multiobjective design optimization for SRMs with a large number of design variables based on a combination of DoE and PSO. A DSD and variance-based sensitivity analysis method was proposed to identify significant design variables to construct the RS models for the subsequent optimization. In the meantime, the design space of the original design optimization problem was reduced. A PSO-based method was proposed to obtain the optimal 3rd-order RS models based on an appropriate fitness evaluation to accurately represent the relationships between the design variables and the machine responses. A method combining the PSO and the optimal 3rd-order RS models was then proposed to solve the multiobjective design optimization problem with the reduced-dimension design space to generate the Pareto front efficiently. Simulation studies were conducted for a sample design of a 6/10 SRM using the proposed optimal design framework as well as the traditional 2nd-order RS model-based and FEA solver-based methods. The results showed that the proposed method has higher accuracy than the traditional 2nd-order RS model-based optimal design methods and can be used for problems with a larger number of design variables. Moreover, compared to the traditional optimal design methods using an FEA solver, the proposed method has a much lower computational cost without sacrificing the accuracy of the design.

References

[1] J. H. Choi, T. H. Kim, K. B. Jang, and J. Lee, "Geometric and electrical optimization design of SR motor based on progressive quadratic response surface method," *IEEE Trans. Magn.*, vol. 39, no. 5, pp. 3241–3243, Sep. 2003.

[2] Y. K. Choi, H. S. Yoon, and C. S. Koh, "Pole-shape optimization of a switched-reluctance motor for torque ripple reduction," *IEEE Trans. Magn.*, vol. 43, no. 4, pp. 1797–1800, Apr. 2007.

[3] F. Sahin, H. B. Ertan, and K. Leblebicioglu, "Optimum geometry for torque ripple minimization of switched reluctance motors," *IEEE Trans. Energy Convers.*, vol. 15, no. 1, pp. 30–39, Mar. 2000.

[4] P. T. Hieu, D. H. Lee, and J. W. Ahn, "Design of 2-phase 4/2 SRM for torque ripple reduction," in *Proc. Int. Conf. Elect. Mach. Syst.*, Oct. 2012, pp. 1–6.

[5] J. Hur, G. H. Kang, J. Y. Lee, J. P. Hong, and B. K. Lee, "Design and optimization of high torque, low ripple switched reluctance motor with flux barrier for direct drive," in *Proc. IEEE IAS Annu. Meeting*, Oct. 2004, pp. 401–408.

[6] C. Ma and L. Qu, "Design considerations of switched reluctance motors with bipolar excitation for low torque ripple applications," in *Proc. IEEE Energy Convers. Congr. Expo.*, Sep. 2013, pp. 926–933.

[7] X. D. Xue, K. W. E. Cheng, T. W. Ng, and N. C. Cheung, "Multi-objective optimization design of in-wheel switched reluctance motors in electric vehicles," *IEEE Trans. Ind. Electron.*, vol. 57, no. 9, pp. 2980–2987, Sep. 2010.

[8] J. Y. Lee, J. H. Chang, D. H. Kang, S. I. Kim, and J. P. Hong, "Tooth shape optimization for cogging torque reduction of transverse flux rotary motor using design of experiment and response surface methodology," *IEEE Trans. Magn.*, vol. 43, no. 4, pp. 1817–1820, Apr. 2007.

[9] X. Gao, T. S. Low, S. Chen, and Z. Liu, "Structural robust design for torque optimization of BLDC spindle motor using response surface methodology," *IEEE Trans. Magn.*, vol. 37, pp. 2814–2817, Jul. 2001.

[10] S. I. Kim, J. P. Hong, Y. K. Kim, H. Nam, and H. I. Cho, "Optimal design of slotless-type PMLSM considering multiple responses by response surface methodology," *IEEE Trans. Magn.*, vol. 42, no. 4, pp. 1219–1222, Apr. 2006.

[11] Y. Kim, S. Member, J. Hong, S. Member, and J. Hur, "Torque characteristic analysis considering the manufacturing tolerance for electric machine by stochastic response surface method," *IEEE Trans. Ind. Appl.*, vol. 39, no. 3, pp. 713–719, May/Jun. 2003.

[12] N. Baatar, H. S. Yoon, M. T. Pham, P. S. Shin, and C. S. Koh, "Shape optimal design of a 9-pole 10-slot PMLSM for detent force reduction using adaptive response surface method," *IEEE Trans. Magn.*, vol. 45, no. 10, pp. 4562–4565, Oct. 2009.

[13] B. N. Cassimere and S. D. Sudhoff, "Population-based design of surface-mounted permanent-magnet synchronous machines," *IEEE Trans. Energy Convers.*, vol. 24, no. 2, pp. 338–346, Jun. 2009.

[14] S. Smaka, S. Konjicija, S. Masic, and M. Cosovic, "Multi-objective design optimization of 8/14 switched reluctance motor," in *Proc. IEEE Int. Elect. Mach. Drives Conf.*, pp. 468–475, May 2013.

[15] T. Raminosoa, B. Blunier, D. Fodorean, and A. Miraoui, "Design and optimization of a switched reluctance motor driving a compressor for a PEM fuel-cell system for automotive applications," *IEEE Trans. Ind. Electron.*, vol. 57, no. 9, pp. 2988–2997, Sep. 2010.

[16] G. G. Wang, "Adaptive response surface method using inherited Latin hypercube design points," *J. Mech. Design*, vol. 125, no. 2, pp. 210–220, Jun. 2003.

[17] J. Kennedy and R. C. Eberhart, *Swarm Intelligence*. San Mateo, CA, USA: Morgan Kaufmann, 2001.

[18] P. Zhang, D. M. Ionel, and N. A. O. Demerdash, "Morphing parametric modeling and design optimization of spoke and V-type permanent magnet machines by combined design of experiments and differential evolution algorithms," in *Proc. IEEE Energy Convers. Congr. Expo.*, pp. 5056–5063, Sep. 2013.

[19] L. Jolly, M. A. Jabbar, and Q. Liu, "Design optimization of permanent magnet motors using response surface methodology and genetic algorithms," *IEEE Trans. Magn.*, vol. 41, no. 10, pp. 3928–3930, Oct. 2005.
[20] Z. L. Gaing, C. H. Lin, M. H. Tsai, M. F. Hsieh, and M. C. Tsai, "Rigorous design and optimization of brushless PM motor using response surface methodology with quantum-behaved PSO operator," *IEEE Trans. Magn.*, vol. 50, no. 1, pp. 1–4, Jan. 2014.
[21] Z. Ren, D. Zhang, and C. S. Koh, "Multi-objective worst-case scenario robust optimal design of switched reluctance motor incorporated with FEM and Kriging," in *Proc. Int. Conf. Elect. Mach. Syst.*, pp. 716–719, Oct. 2013.
[22] Y. Duan and D. M. Ionel, "A review of recent developments in electrical machine design optimization methods with a permanent-magnet synchronous motor benchmark study," *IEEE Trans. Ind. Appl.*, vol. 49, no. 3, pp. 1268–1275, May/Jun. 2013.
[23] R. Krishnan, *Switched Reluctance Motor Drives*. Boca Raton, FL, USA: CRC Press, 2001.
[24] J. Faiz, B. Ganji, C.E. Carstensen, K.A. Kasper, and R.W. De Doncker, "Temperature rise analysis of switched reluctance motors due to electromagnetic losses," *IEEE Trans. Magn.*, vol. 45, no. 7, pp. 2927–2934, Jul. 2009.
[25] R. Arumugam, J. F. Lindsay, and R. Krishnan, "Sensitivity of pole arc/pole pitch ratio on switched reluctance motor performance," in *Proc. IEEE IAS Annu. Meeting*, Oct. 1988, vol. 1, pp. 50–54.
[26] J. Faiz and J. W. Finch, "Aspects of design optimization for switched reluctance motors," *IEEE Trans. Energy Convers.*, vol. 8, no. 4, pp. 704–713, Dec. 1993.
[27] N. K. Sheth and K. R. Rajagopal, "Optimum pole arcs for a switched reluctance motor for higher torque with reduced ripple," *IEEE Trans. Magn.*, vol. 39, no. 5, pp. 3214–3216, Sep. 2003.
[28] A. Saltelli, M. Ratto, T. Andres, F. Campolongo, J. Cariboni, D. Gatelli, M. Saisana, and S. Tarantola, *Global Sensitivity Analysis: The Primer*. Hoboken, NJ, USA: Wiley, 2008.
[29] B. Jones and C. Nachtsheim, "A class of three-level designs for definitive screening in the presence of second-order effects," *J. Quality Tech.*, vol. 43, no. 1, pp. 1–15, Jan. 2011.
[30] J. P. Hong, K. H. Ha, and J. Lee, "Stator pole and yoke design for vibration reduction of switched reluctance motor," *IEEE Trans. Magn.*, vol. 38, no. 2, pp. 929–932, Mar. 2002.
[31] B. Bilgin, A. Emadi, and M. Krishnamurthy, "Design considerations for switched reluctance machines with a higher number of rotor poles," *IEEE Trans. Ind. Electron.*, vol. 59, no. 10, pp. 3745–3756, Oct. 2012.
[32] T.J.E. Miller, "Optimal design of switched reluctance motors," *IEEE Trans. Ind. Electron.*, vol. 49, no. 1, pp. 15–27, Feb. 2002.
[33] F. Fuerle and J. Sienz, "Formulation of the Audze-Eglais uniform Latin hypercube design of experiments for constrained design spaces," *Adv. Eng. Softw.*, vol. 42, pp. 680–689, Sep. 2011.
[34] F. A. C. Viana, G. Venter, and V. Balabanov, "An algorithm for fast optimal Latin hypercube design of experiments," *Int. J. Numer. Meth. Eng.*, vol. 82, pp. 135–156, Apr. 2010.
[35] R. H. Myers, D. C. Montgomery, and C. M. Anderson-Cook, *Response Surface Methodology: Process and Product Optimization Using Designed Experiments*. Hoboken, NJ, USA: Wiley, 2009.
[36] A. E. Smith and D. W. Coit, "Constraint-handling techniques-penalty functions," in *Handbook of Evolutionary Computation*. Bristol, U.K.: Inst. of Physics/Oxford Univ. Press, 1997, Chapter C5.2.

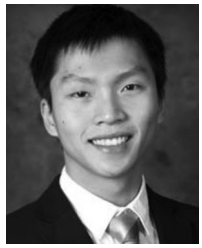

Cong Ma (S'13) received the B.Eng. degree in electrical engineering from Shandong University, Jinan, China, in 2012. He is currently working toward the Ph.D. degree in electrical engineering at the University of Nebraska–Lincoln, Lincoln, NE, USA.

His research interests include electrical machine design, design optimization, modeling and analysis of electric machines, and motor drives.

Mr. Ma is a Member of Eta Kappa Nu.

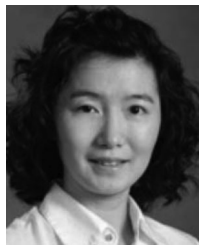

Liyan Qu (S'05–M'08) received the B.Eng. (with the highest distinction) and M.Eng. degrees in electrical engineering from Zhejiang University, Hangzhou, China, in 1999 and 2002, respectively, and the Ph.D. degree in electrical engineering from the University of Illinois at Urbana–Champaign, Champaign, IL, USA, in 2007.

From 2007 to 2009, she was an Application Engineer with Ansoft Corporation, Irvine, CA, USA. Since January 2010, she has been with the University of Nebraska—Lincoln, Lincoln, NE, USA, where she is currently an Assistant Professor in the Department of Electrical and Computer Engineering. Her research interests include energy efficiency, renewable energy, numerical analysis and computer-aided design of electric machinery and power electronic devices, dynamics and control of electric machinery, permanent-magnet machines, and magnetic materials.